



*Citation for published version:*

Kuenzel, C, Zhang, F, Ferrandiz-Mas, V, Cheeseman, CR & Gartner, EM 2018, 'The mechanism of hydration of MgO-hydromagnesite blends', *Cement and Concrete Research*, vol. 103, pp. 123-129.  
<https://doi.org/10.1016/j.cemconres.2017.10.003>

*DOI:*

[10.1016/j.cemconres.2017.10.003](https://doi.org/10.1016/j.cemconres.2017.10.003)

*Publication date:*

2018

*Document Version*

Peer reviewed version

[Link to publication](#)

## University of Bath

### Alternative formats

If you require this document in an alternative format, please contact:  
[openaccess@bath.ac.uk](mailto:openaccess@bath.ac.uk)

#### General rights

Copyright and moral rights for the publications made accessible in the public portal are retained by the authors and/or other copyright owners and it is a condition of accessing publications that users recognise and abide by the legal requirements associated with these rights.

#### Take down policy

If you believe that this document breaches copyright please contact us providing details, and we will remove access to the work immediately and investigate your claim.

# The mechanism of hydration of MgO-hydromagnesite blends

C. Kuenzel, F. Zhang, <sup>a</sup>V. Ferrándiz-Mas, C.R. Cheeseman\*, E.M. Gartner

Department of Civil and Environmental Engineering, Imperial College London,  
South Kensington Campus, London SW7 2AZ, United Kingdom,

<sup>a</sup> Department of Architecture and Civil Engineering, University of Bath, BA2 7AY, United Kingdom

\*Corresponding author: Email: c.cheeseman@imperial.ac.uk

## ABSTRACT

The hydration of reactive periclase (MgO) in the presence of hydromagnesite ( $\text{Mg}_5(\text{CO}_3)_4(\text{OH})_2 \cdot 4\text{H}_2\text{O}$ ) was investigated by a variety of physical and chemical techniques. Hydration of pure MgO-water mixtures gave very weak pastes of brucite ( $\text{Mg}(\text{OH})_2$ ), but hydration of MgO-hydromagnesite blends gave pastes which set quickly and gave compressive strengths of potential interest for construction applications. The strengths of the blends increased with hydration time at least up to 28 days, and were not significantly decreased by increasing the hydromagnesite content up to 30%. Raman spectroscopy suggests that an amorphous phase, of composition between that of brucite, hydromagnesite and water, may form. Small amounts of calcite also form due to CaO in the MgO source. Thermodynamic calculations imply that the crystalline phase artinite ( $\text{MgCO}_3 \cdot \text{Mg}(\text{OH})_2 \cdot 3\text{H}_2\text{O}$ ) should be the stable product in this system, but it is not observed by either XRD or FTIR techniques, which suggests that its growth may be kinetically hindered.

**Keywords:** MgO, cement, hydration, hydromagnesite, artinite, brucite,

## 1. Introduction

MgO (periclase) reacts with water to give brucite ( $\text{Mg}(\text{OH})_2$ ) under conditions relevant to normal construction materials. The rate of reaction increases as the crystallinity of the periclase decreases (i.e. smaller mean crystallite size). Periclase is usually manufactured by calcination (decarbonation) of magnesite ( $\text{MgCO}_3$ ) that is obtained from natural mineral deposits. The lower the decarbonation temperature, the lower the degree of crystallinity of the resulting periclase. Lightly-burned magnesite is of particular interest for use in hydraulic cements because it reacts very rapidly with water [1].

The hydration of MgO has been extensively studied [2-6]. Water molecules, even from the vapour phase, react rapidly with the anhydrous MgO surface to form a surface layer of  $\text{Mg}(\text{OH})_2$ , but with a structure probably significantly different from that of brucite due to interactions with the underlying oxide. This surface hydrate displays an apparent solubility somewhat higher than pure brucite. Thus, at high relative

39 humidity, when significant amounts of physically adsorbed water, or excess liquid water, is present, this  
40 hydrated surface layer can dissolve in the mobile water layer and reprecipitate as brucite crystallites  
41 further away from the surface. The hydrated surface layer on the oxide is continually reformed by further  
42 reaction of the underlying oxide with water. The hydration rate of MgO is effectively limited by the rate  
43 at which the  $\text{Mg}(\text{OH})_2$  layer on the surface of the MgO dissolves in the water layer. This in turn is  
44 influenced by the rate at which dissolved  $\text{Mg}^{++}$  and  $\text{OH}^-$  ions are removed from the water layer by, for  
45 example, precipitation.

46

47 Periclase can also react with  $\text{CO}_2$  in the presence of water (liquid or vapour) to give hydrated carbonates  
48 or hydroxy-carbonates such as nesquehonite ( $\text{MgCO}_3 \cdot 3\text{H}_2\text{O}$ ) and hydromagnesite ( $\text{Mg}_5(\text{CO}_3)_4$   
49  $(\text{OH})_2 \cdot 4\text{H}_2\text{O}$ ). It is reported that nesquehonite forms readily from aqueous solutions at ambient  
50 temperature [9,10]. Table 1 lists the known phases in the MgO- $\text{CO}_2$ - $\text{H}_2\text{O}$  system under conditions of  
51 interest, and gives standard free energies of formation from the elements at  $25^\circ\text{C}$  [7, 8]. From this data  
52 it can be shown that under ambient atmospheric conditions, all hydrated magnesium (hydroxy-)  
53 carbonates should convert to magnesite. However, the kinetics of magnesite growth is very slow,  
54 especially below  $100^\circ\text{C}$ , and so the hydrated carbonates and hydroxy-carbonates, which have much  
55 higher growth rates, usually form and do not convert substantially to magnesite over decades under  
56 typical exposure conditions for construction materials [11].

57

58 Sealed samples of pure pastes of reactive MgO and water do not gain any significant compressive  
59 strength, despite the formation of brucite. Moreover, if such pastes are left in the open air, they only  
60 carbonate very slowly and do not harden (unlike pastes made of lime, which harden rapidly by  
61 atmospheric carbonation - the basis of the lime mortar technology used for many millennia). For this  
62 reason, MgO has not until recently been considered of value in simple binders except when significant  
63 amounts of other inorganic chemicals are added (e.g. chlorides, sulfates, or phosphates: to make  
64 magnesium oxy-chloride, magnesium oxy-sulfate or magnesium phosphate cements, respectively).  
65 However, over the last decade or so, there has been increasing interest in using MgO in silicate-based  
66 binder system, or in carbonated binders. Blends of MgO with Portland cement, granulated blast furnace  
67 slag (GBFS) or coal fly ash (FA) have been studied to produce low-carbon hydraulic binders [1-5,9].  
68 However, there is little evidence for significant contribution of MgO hydration to the strength  
69 development of such cements. MgO hydration is also known to cause harmful expansion in Portland  
70 cement concretes [10] under certain conditions. Moreover, the fact that conventional MgO production  
71 methods are very energy and  $\text{CO}_2$  intensive makes it difficult to justify the use of MgO in low-carbon  
72 hydraulic cements [12]. A more promising approach for  $\text{CO}_2$  emissions reduction is to use MgO in  
73 cements that hardens by carbonation, [6-8], but even then, only a fraction of the  $\text{CO}_2$  released during  
74 manufacture is recaptured. The most desirable approach would be to use MgO derived from natural  
75 magnesium silicate raw materials by a new low-energy route, as first proposed by Vlasopoulos [13], but

76 no practical low-energy production process for achieving this goal yet exists [12]. However, developing  
77 such a process remains an important long-term research goal.

78  
79 A significant advance in developing low-carbon hydraulic cements based on MgO was made in 2009,  
80 when the addition of hydrated magnesium carbonates was found to significantly change the hydration  
81 of MgO, resulting in pastes that rapidly set and developed significant strength [14-16]. These findings  
82 were unexpected and novel [19]. The results have been confirmed for mixtures containing  
83 hydromagnesite (HY) as the additive at up to 50% MgO replacement levels [14-16]. The fact that  
84 cements made from such mixtures contain significant levels of carbonate is the key to reducing the  
85 carbon footprint [12]. The addition of HY reportedly results in more rapid and extensive dissolution of  
86 MgO and the precipitation of Mg(OH)<sub>2</sub> in the form of very small interlocking crystallites with different  
87 morphology from that formed when just MgO is hydrated[16]. However, the reason for this change in  
88 morphology, and how it leads to strength development, is still unclear. An improved understanding of  
89 the hydration reaction mechanism is essential if these magnesium hydroxy-carbonate cements are to be  
90 further developed and optimised. This paper reports on a systematic investigation into the hydration  
91 reactions of MgO in the presence of hydromagnesite in order to improve understanding of the hydration  
92 mechanism and strength development.

## 94 **2. Materials and Methods**

### 96 **2.1 Materials**

97 A commercial MgO powder prepared by calcining magnesite at 900°C (Baymag 30, Baymag Inc.,  
98 Alberta, Canada) and technical grade hydromagnesite (Calmag CALMAGS GmbH, Germany) were  
99 used in all experiments. The chemistry of the raw materials is given in Table 2. XRF results are presented  
100 as total mass percentage of non-volatile elemental oxides in the material (i.e. on an ignited basis.) The  
101 measured and expected loss on ignition (LoI) data are included to demonstrate the purity of each powder.  
102 The particle size distribution of the as-received raw materials are given in Fig. 1.

### 104 **2.2 Preparation of samples**

105 MgO and HY were mixed at mass ratios of 9:1, 8:2 and 7:3. Water was added to form pastes using the  
106 recommended mixing method for mortar and pastes [17]. A water/total solids mass ratio of 0.62 was  
107 used in all samples. This was the minimum water content that allowed formation of a homogenous paste  
108 in all cases, although increasing the hydromagnesite content always increased paste viscosity. Pastes  
109 were cast into 50 x 10 x 10 mm rectangular moulds and vibrated for 5 minutes to remove air bubbles.  
110 They were then covered with a glass plate to prevent moisture loss and limit reaction with atmospheric  
111 CO<sub>2</sub>, and allowed to hydrate for 24 hours at 22 ± 1°C. The samples were then de-moulded and stored in  
112 deionised water at 22 ± 1°C for periods up to 56 days.

### 114 **2.3** *Physical/chemical properties*

115 The heat of hydration of trial mixes was monitored by isothermal conduction calorimetry (Wexham  
116 Developments Ltd, UK). The bath temperature was set at  $20.0 \pm 0.1^\circ\text{C}$  and 25g of paste samples with  
117 0.62 w/s ratio were mixed by hand for 2 minutes before being placed in the calorimeter. The time  
118 between the start of mixing and obtaining the first calorimetry data point was ~10 minutes.

119

120 Cured cast samples were removed from the water bath, cut in half to give 25 x 10 x 10 mm prisms and  
121 immediately tested in uniaxial compression, parallel to the long axis at a constant loading rate of 0.08  
122 kN/s (ADR Auto strength machine, ELE International, UK) to give compressive strength data.  
123 Preliminary tests demonstrated that this non-standard test procedure gave highly reproducible results.

124

125 The pH of slurry samples made with a w/s ratio of 3 was determined using an Inlab Routine Pro  
126 electrode, (Mettler Toledo, Switzerland). The slurry was continuously stirred while **exposed to the**  
127 **atmosphere**, and the pH measured at various times throughout the hydration process at  $22 \pm 1^\circ\text{C}$ .

128

### 129 **2.4** *Microstructural and phase analysis*

130 Powder x-ray diffraction (XRD) using Cu K $\alpha$  radiation in the range of 5 to 65° 2 $\theta$  was used to semi-  
131 quantitatively compare the relative amounts of crystalline phases in paste samples (X-Pert PRO MPD,  
132 PANalytical, Netherlands). Fourier transform infrared spectroscopy (FTIR) was used to detect  
133 additional phases in the reaction products. Brucite control samples were prepared by hydrating MgO  
134 (Baymag 30) in distilled water. Raman spectrometry (Renishaw inVia Raman Microscope, UK) was  
135 used to characterise the different MgO/HY mixes. The microstructures of the as-received powder  
136 materials and hydrated, fractured MgO/HY samples were analysed using scanning electron microscopy  
137 (SEM, JEOL JSM 5610, Japan). SEM samples were gold coated using a current of 20 mA.

138

139 Prior to analysis the paste samples were ground with acetone in a mortar and pestle to inhibit further  
140 hydration. This is an accepted way to inhibit hydration of calcium silicate-based cements as hydration  
141 water is replaced by acetone [18]. The slurry formed was then filtered and rinsed with additional acetone  
142 using vacuum filtration and the solid residue dried at 60 °C to constant weight.

143

## 144 **3. Results**

145

### 146 **3.1** *Physical properties*

147 Isothermal conduction calorimetry power output and total heat evolution curves for pastes of pure MgO  
148 and a 9:1 MgO: HY blend are shown in Fig. 2. The inclusion of 10% HY greatly accelerates the early  
149 hydration compared to pure MgO paste. Hydration occurs prior to obtaining the first calorimetry data  
150 point. Both samples show an acceleration period followed by a reducing rate of hydration, suggesting a  
151 nucleation and growth process in which the added HY acts as growth sites for hydrates. The maximum

152 hydration rate occurs after about 10 hours for pure MgO and 2 hours for the sample with 10% HY. The  
153 total heat curves may not be very accurate due to the loss of heat in the first few minutes, due to external  
154 mixing, and the well-known problem of calibration and baseline drift in long-term isothermal  
155 calorimetry experiments, but they appear to indicate that the pure MgO hydrates to a significantly greater  
156 extent than the MgO in the 9:1 blend over the one week (168 hours) period shown. Thermodynamic data  
157 bases give a heat of hydration of MgO of about 930 J/g [19], so the total heat evolution data suggests  
158 that pure MgO is only about 50% hydrated after one week, and the blended MgO is even less hydrated.  
159

160 Fig. 3 shows the variation in solution pH over 28 days for w/s = 3 slurries of pure MgO, pure HY and a  
161 9:1 MgO: HY mixture. Slurries made with 8:2 and 7:3 MgO: HY mixtures gave similar results to the  
162 9:1 mixture, so the data for these are not shown. The initial pH value for the pure MgO and the MgO:  
163 HY mixtures was about 12.4 whereas for pure HY it was close to 10. The pure MgO slurry shows a slow  
164 reduction in pH with time, reaching a value of about 11.2 after one week, whereas MgO: HY mixes all  
165 showed a much more rapid decrease in pH, reaching values close to, or even slightly below, those of  
166 pure HY after ~1 day.  
167

168 Table 3 shows that all three MgO-HY paste samples give very similar compressive strength  
169 development, achieving about 18 MPa after 7 days, and increasing to about 24 MPa at 28 days. Pure  
170 MgO pastes did not give sufficient strength for sample demoulding and so cannot be compared directly  
171 in the table.  
172

### 173 **3.2 Microstructural and phase analyses**

174 The XRD scans shown in Fig. 4 are only semi-quantitative, as there were no internal standard. However,  
175 given that the sample preparation and analysis techniques were quite repeatable, comparisons of peak  
176 intensities seem justifiable as a way of examining changes in the relative amounts of the main crystalline  
177 phases present. In the pure system, (Fig. 4b) periclase disappears (dissolves) with time while brucite  
178 forms (precipitates). Even after 28 days of hydration, the periclase peak in the pure system has not  
179 completely disappeared. A weak peak in Fig. 4a also indicates the formation of some calcite (CaCO<sub>3</sub>).  
180 CaO is an impurity in the MgO that carbonates by reaction with atmospheric CO<sub>2</sub>.  
181

182 The reactions of MgO: HY blends show similar trends as a function of hydration time, with the  
183 disappearance of periclase and formation of brucite, but at different rates, as clearly shown in Fig 4c for  
184 pure MgO and 9:1 MgO: HY pastes hydrated for 28 days. Significantly more MgO appears to have  
185 hydrated and more Mg(OH)<sub>2</sub> has formed in the pure paste than in the 9:1 blend. In addition, the Mg(OH)<sub>2</sub>  
186 peak in the 9:1 blend is significantly broader than in the pure system, suggesting a smaller mean  
187 crystallite size [20]. This is in agreement with calorimetry data, where MgO does not fully hydrate to  
188 brucite.  
189

190 In the XRD data for MgO: HY blends, HY peaks were observed mainly for samples with MgO: HY  
191 ratios of 8:2 and 7:3 but hardly at all for the 9:1 samples due to the low concentration of HY and the  
192 corresponding weak diffraction peaks. Mg(OH)<sub>2</sub> and MgO were always present, as expected, and the  
193 Mg(OH)<sub>2</sub> peak always shows significant broadening compared to those found in the pure system. No  
194 additional peaks are observed, so any other phases which might be present must be effectively x-ray  
195 amorphous.

196

197 The FTIR spectra of samples produced by hydrating MgO, HY and the MgO: HY 70:30 mix for 28 days  
198 are shown in Fig. 5. The MgO: HY mixes with ratios of 90:10 and 80:20 are not shown because HY is  
199 only present in small quantities and the corresponding bands are too weak to observe [21]. Several bands  
200 can be detected which have been characterised in previous studies, as shown in Table 4. All the bands  
201 identified are seen in the spectra for the three samples containing HY, except for that due to O-H bonds  
202 in Mg(OH)<sub>2</sub> at 3700 cm<sup>-1</sup> which are, as expected, not observed in the pure HY sample. Small amounts  
203 of carbonate are observed in hydrated MgO. This is consistent with the XRD data and confirms that the  
204 MgO reacts with atmospheric CO<sub>2</sub> over time, although the carbonate ions detected in this case are  
205 probably mainly present as CaCO<sub>3</sub>. The presence of carbonate impurities in brucite (Mg(OH)<sub>2</sub>) has  
206 previously been reported in FTIR studies [22]. Previous research has shown that for pure magnesite,  
207 (MgCO<sub>3</sub>), a single asymmetric stretching band is observed between 1478 and 1450 cm<sup>-1</sup>. The presence  
208 of two bands in the 1420-1480 cm<sup>-1</sup> region, as in HY, indicates the presence of two different carbonate  
209 ion environments [21, 23, 24]. The HY signal at ~600cm<sup>-1</sup> is unassigned, although this band has been  
210 observed by other researchers [25]. Studies on the dehydration and rehydration of HY have also  
211 identified a band at ~2350cm<sup>-1</sup> which has been assigned either to a CO<sub>2</sub> inclusion or a terminal CO<sub>2</sub>,  
212 corresponding to the ν<sub>3</sub> fundamental of CO<sub>2</sub> [25, 26]. However, this band cannot be measured in our  
213 study, probably due to the background noise level.

214

215 Raman spectroscopy was used to search for other phases not ‘visible’ using FTIR. Fig. 6 shows the  
216 Raman spectra of pure HY, hydrated MgO, hydrated MgO: HY samples with ratios of 9:1 and 7:3. All  
217 samples had been cured for 28 days. Three main peaks at 280 cm<sup>-1</sup>, 440 cm<sup>-1</sup> and 1100 cm<sup>-1</sup> can be  
218 identified. The peaks at 280 cm<sup>-1</sup> and 440 cm<sup>-1</sup> observed in the hydrated MgO sample also appear in the  
219 other spectra except for the spectrum of HY. These two peaks are related to Mg(OH)<sub>2</sub> [27]. The peak at  
220 ~1120cm<sup>-1</sup> is due to symmetrical stretching of the CO<sub>3</sub><sup>2-</sup> ion, [28, 29], which is why it is much stronger  
221 in Raman spectra. However, of more interest is the formation of a broad weak peak or series of small  
222 peaks between 1050 and 1120 cm<sup>-1</sup> for MgO: HY mixes. These peaks are not seen for pure MgO and  
223 HY and are probably due to symmetrical stretching of CO<sub>3</sub><sup>2-</sup> in other magnesium carbonate phases,  
224 which could be very poorly crystalline. Table 5 lists a number of possible phases with peaks in this  
225 range.

226

227 Fig. 7 shows SEM images of hydrated MgO and HY and fracture surfaces of pastes cured for 7 and 28  
228 days. Fig. 7 (c, d, e and f) show that over time well-developed crystalline morphologies (plates) are  
229 formed. These are not observed either in hydrated pure MgO or in pure HY samples.

230

#### 231 4. Discussion

232

233 The initial rate of hydration of MgO is strongly increased by HY, which suggests that HY additions  
234 provide additional growth sites for the hydrates (Mg(OH)<sub>2</sub> and probably other x-ray amorphous hydrate  
235 phases) promoting further MgO hydration [13]. It was expected that pure MgO would fully hydrate to  
236 Mg(OH)<sub>2</sub>, but this was not shown by calorimetry or XRD. This incomplete hydration is probably due to  
237 a brucite layer forming on the MgO particle surface that inhibits water reaching unreacted MgO by  
238 acting as a passivation layer. However, it is expected that eventually pure MgO will fully hydrate to  
239 Mg(OH)<sub>2</sub>. Of particular interest is the high initial pH of 12.4 for MgO and MgO: HY systems when  
240 mixed with water, because a pH of ~10 had been expected. The measured pH is actually close to that of  
241 a saturated portlandite (Ca(OH)<sub>2</sub>) solution, leading to the conclusion that CaO impurities in the MgO  
242 and HY cause the high initial pH. The pH of the pure MgO slurry then falls slowly with time due to  
243 atmospheric carbonation to produce calcite, consistent with XRD observations of calcite in the system.  
244 When MgO is mixed with HY, the pH falls much more rapidly, which can be explained by HY  
245 containing readily soluble carbonate ions which are capable of neutralizing Ca(OH)<sub>2</sub> much more rapidly  
246 than CO<sub>2</sub> from the atmosphere. Rapid precipitation of calcite at early ages due to reaction with HY could  
247 provide another source of nucleation sites for hydration products of MgO and **the formation of CaCO<sub>3</sub>**  
248 **may also contribute to rapid setting and compressive strength development.**

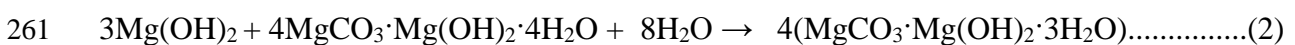
249

250 After the first peak in the calorimetry data, the rate of heat evolution is significantly lower for the MgO:  
251 HY blends, and the XRD data confirm that the amount of unreacted MgO is higher in these blends at  
252 later ages than in the pure system, despite the fact that blends give far higher compressive strengths.  
253 This suggests that additional hydrates produced in the blends have a retarding effect on the later  
254 hydration of MgO. The effect might be due to surface blocking or to the formation of diffusion barriers.  
255 These additional hydrates are also presumed to be responsible for strength development.

256

257 Table 1 gives the free energies of the known crystalline phases of interest in this system. Artinite  
258 {MgCO<sub>3</sub>·Mg(OH)<sub>2</sub>·3H<sub>2</sub>O} is intermediate in composition between Mg(OH)<sub>2</sub> and HY and can, in  
259 principle, be formed from these two phases and water by the following reaction:

260



262

263 A calculation using the thermodynamic data from Table 1 gives the free energy change of the reaction  
264 as -6.42 kJ/mol, which implies that the equilibrium should lie on the right-hand side at 25°C. Thus,



265 artinite should form in MgO: HY blends. However, it is not detected in the XRD data. This could be  
266 due to weak XRD peaks or it could be due to a very low degree of crystallinity. Artinite has a carbonate  
267 symmetric stretching peak at  $1092\text{ cm}^{-1}$  (Table 5) which should be observable in both IR and Raman  
268 spectra. No such peak is visible in the FTIR spectra of MgO: HY blends (Fig. 5) but it could be too weak  
269 to detect. The Raman spectra of hydrated MgO: HY blends (Fig. 6) show a very broad peak between  
270 about  $1040$  and  $1120\text{ cm}^{-1}$  which suggests a disordered hydroxy-carbonate phase that might not be too  
271 far from artinite in composition. It thus seems possible that some kind of amorphous hydroxy-carbonate,  
272 intermediate in composition between HY and brucite, may form in MgO: HY pastes and be responsible  
273 for high compressive strengths relative to pure MgO pastes.

274

275 The SEM images in Fig. 7 neither confirm nor deny the hypothesis of a new phase in MgO: HY pastes.  
276 It is notable that quite large ( $\sim 5\mu\text{m}$ ) platy crystals are formed after 28 days in the 9:1 MgO: HY paste.  
277 These could be  $\text{Mg}(\text{OH})_2$ , but they are much larger than the crystals observed in pure MgO. Moreover,  
278 the XRD peak broadening of brucite observed in the MgO: HY blends would tend to suggest smaller,  
279 rather than larger, crystals. It is therefore possible that these crystals are the new phase, in which case  
280 the poor x-ray crystallinity is due to either being very thin in the direction perpendicular to the basal  
281 plane, or possibly to some other kind of internal disorder.

282

## 283 5. Conclusions

284

285 Addition of hydromagnesite, (HY,  $\text{Mg}_5(\text{CO}_3)_4(\text{OH})_2 \cdot 4\text{H}_2\text{O}$ ), significantly accelerates the hydration of  
286 reactive periclase (MgO) in pastes. The hydration of pure MgO gives very weak pastes despite fairly  
287 rapid formation of brucite ( $\text{Mg}(\text{OH})_2$ ), but the addition of HY at MgO at replacement dosages of 10-  
288 30% results in pastes that give significant compressive strengths, despite the absence of significant  
289 increases in the apparent degree of hydration of the MgO. Evidence from pH measurements also  
290 suggests that carbonate ions from HY can combine rapidly in solution with calcium ions released by  
291 CaO, (an impurity in the MgO source,) to precipitate small amounts of calcite at early ages. This might  
292 also contribute to an acceleration of the hardening reactions, perhaps by acting as nucleation sites.

293

294 Analyses of the hydrated pastes by XRD and FTIR techniques do not clearly show any new MgO-based  
295 phases, but there is a broad but weak Raman peak at  $1120$ - $1040\text{ cm}^{-1}$  that could represent a new  
296 amorphous phase. It is thus concluded that if any new cohesive phase forms in this system, it is probably  
297 X-ray amorphous with a composition roughly intermediate between that of HY and brucite. A  
298 thermodynamic calculation suggests that artinite ( $\text{MgCO}_3 \cdot \text{Mg}(\text{OH})_2 \cdot 3\text{H}_2\text{O}$ ) should form-be a stable  
299 product phase during the hydration of MgO:-HY blends, but the fact that it is not observed by XRD or  
300 FTIR suggests that its formation may be kinetically hindered.

301

302 The formation of an amorphous phase intermediate in composition between ~~HY<sub>2</sub>~~ and Mg(OH)<sub>2</sub> and  
303 water is a possible explanation for the surprisingly high strengths produced by hydrating MgO: HY  
304 blends, compared to the very low strengths produced by hydration of pure MgO. Such a phase must  
305 have a high degree of cohesion.

306  
307 These results hold promise for the development of improved binders in the magnesium-hydroxy-  
308 carbonate system. Such binders have the potential to reduce carbon emissions from manufacturing  
309 construction materials, provided that MgO can be obtained from magnesium silicates by an energy-  
310 efficient process. However, there are currently many aspects of hydration and strength development in  
311 this system that remain unclear.

### 312 313 **Acknowledgement**

314 F. Zhang acknowledges the support of an EPSRC Case Award sponsored by Laing O'Rourke.

### 315 316 **References**

- 317
- 318 1. Birchal, V.S.S., S.D.F. Rocha, and V.S.T. Ciminelli, *The effect of magnesite calcination conditions*  
319 *on magnesia hydration*. Minerals Engineering, 2000. **13**(14-15): p. 1629-1633.
  - 320 2. Birchal, V.S.S., S.D.F. Rocha, M.B. Mansur, and V.S.T. Ciminelli, *A simplified mechanistic*  
321 *analysis of the hydration of magnesia*. The Canadian Journal of Chemical Engineering, 2001. **79**:  
322 p. 507-511.
  - 323 3. Feitknecht, W. and H. Braun, *Der Mechanismus der Hydratation von Magnesiumoxid mit*  
324 *Wasserdampf*. Helvetica Chimica Acta, 1967. **80**.
  - 325 4. Glasson, D.R., *Reactivity of lime and related oxides (Part VII) - Production of activated lime and*  
326 *magnesia*. Journal of Applied Chemistry, 1963. **13**: p. 111-118.
  - 327 5. Maryska, M. and J. Blaha, *Hydration kinetics of magnesium oxide: Part 3 hydration rate of MgO*  
328 *in terms of temperature and time of its firing*. Ceramics - Sillicaty, 1997. **41**: p. 121-123.
  - 329 6. Smithson, G.L. and N.N. Bakhshi, *The kinetics and mechanism of the hydration of magnesium oxide*  
330 *in a batch reactor*. The Canadian Journal of Chemical Engineering, 1969. **47**: p. 508-513.
  - 331 7. Dean, J.A., *Lange's Handbook of Chemistry*. 15 ed. 1999, New York, USA: McGraw-Hill.
  - 332 8. Hänchen, M., V. Prigiobbe, R. Baciocchi, and M. Mazzotti, *Precipitation in the Mg-carbonate*  
333 *system—effects of temperature and CO<sub>2</sub> pressure*. Chemical Engineering Science, 2008. **63**: p.  
334 1012–1028.
  - 335 9. Zhao, L., L. Sang, J. Chen, J. Ji, and H.H. Teng, *Aqueous carbonation of natural brucite, relevance*  
336 *to CO<sub>2</sub> sequestration*. Environmental Science Technology, 2010. **44**: p. 406-411.
  - 337 10. Xiong, Y.L. and A.S. Lord, *Experimental investigation of the reaction path in the MgO-CO<sub>2</sub>-H<sub>2</sub>O*  
338 *system in solution with various ionic strength and their applications in nuclear waste isolation*.  
339 *Applied Geochemistry*, 2008. **23**(6): p. 1634-1659.

- 340 11. Saldi, G.D., G. Jordan, J. Schott, and E.H. Oelkers, *Magnesite growth rate as a function of*  
341 *temperature and saturation state*. *Geochimica et Cosmochimica Acta*, 2009. **73**: p. 5646-5657.
- 342 12. Gartner, E. and T. Sui, *Alternative cement clinkers*. *Cement and Concrete Research*, 2017 (in press  
343 - available online.)
- 344 13. Vlasopoulos, N., *Waste minimisation through sustainable magnesium oxide cement products*, in  
345 *Civil and Environmental Engineering*. 2007, Imperial College London: London.
- 346 14. Flatt, R.J., N. Roussel, and C.R. Cheeseman, *Concrete: an eco material that needs to be improved*.  
347 *Journal of European Ceramic Society*, 2012. **32**: p. 2787-2798.
- 348 15. Devaraj, A.R., H.X. Lee, D.A.M. Velandia, and N. Vlasopoulos, *Binder Composition*. 2011: US  
349 20140290535 A1.
- 350 16. Vlasopoulos, N. and C.R. Cheeseman, *Binder composition*. 2009: US Patent 8496751 B2.
- 351 17. BS, *EN 196-1 Methods of testing cements - Determination of strength*. 2005.
- 352 18. Collier, N.C., J.H. Sharp, N.B. Milestone, J. Hill, and I.H. Goffrey, *The influence of water removal*  
353 *techniques on the composition and microstructure of hardened cement pastes*. *Cement and*  
354 *Concrete Research*, 2008. **38**: p. 737-744.
- 355 19. Thomas, J.J., S. Musso, and I. Prestini, *Kinetics and activation energy of magnesium oxide*  
356 *hydration*. *Journal of the American Ceramic Society*, 2014. **97**(1): p. 275-282.
- 357 20. Navarro, C.R., F.E. Hansen, and W.S. Ginnell, *Calcium hydroxide crystal evolution upon ageing*  
358 *of lime putty*. *Journal of American Ceramic Society*, 1998. **81**: p. 3032-3034.
- 359 21. Bruni, S., F. Cariati, P. Fermo, A. Pozzi, and L. Toniolo, *Characterization of ancient magnesian*  
360 *mortars coming from northern Italy*. *Thermochimica Acta*, 1998. **321**: p. 161-165.
- 361 22. Frost, R.L. and J.T. Kloprogge, *Infrared emission spectroscopic study of brucite*. *Spectrochimica*  
362 *Acta Part A: Molecular and Biomolecular Spectroscopy*, 1999. **55**: p. 2195-2205.
- 363 23. Choudhari, B.P., M.C. Vaidya, and D.S. Datar, *Physico-chemical studies on basic magnesium*  
364 *carbonates*. *Indian Journal of Chemistry*, 1972. **10**: p. 731-733.
- 365 24. Sawada, Y., J. Yamaguchi, O. Sakurai, K. Uematsu, N. Mizutani, and M. Kato, *Thermal*  
366 *decomposition of basic magnesium carbonates under high-pressure gas atmospheres*.  
367 *Thermochimica Acta*, 1979. **32**: p. 277-291.
- 368 25. Botha, A. and C.A. Strydom, *DTA and FT-IR analysis of the rehydration of basic magnesium*  
369 *carbonate*. *Journal of Thermal Analysis and Calorimetry*, 2003. **71**: p. 987-995.
- 370 26. Schrader, B., *Infrared and Raman spectroscopy: methods and applications*. 1989, London: Wiley.
- 371 27. Buchanan, R.A., H.H. Caspers, and J. Murphy, *Lattice Vibration Spectra of Mg(OH)<sub>2</sub> and*  
372 *Ca(OH)<sub>2</sub>*. *Applied Optics*, 1963. **2**(11): p. 1147-1150.
- 373 28. Edwards, H.G.M., S.E. Jorge Villar, J. Jehlicka, and T. Munshi, *FT-Raman spectroscopic study of*  
374 *calcium-rich and magnesium-rich carbonate minerals*. *Spectrochimica Acta Part A*, 2005. **61**: p.  
375 2273-2280.
- 376 29. Scheetz, B.E. and W.B. White, *Vibrational spectra of the alkaline earth double carbonates*.  
377 *American Mineralogist*, 1977. **62**: p. 39-50.

- 378 30. Han, H., S. Hu, J. Feng, and H. Gao, *Effect of stearic acid, zinc stearate coating on the properties*  
379 *of synthetic hydromagnesite*. Applied Surface Science, 2011. **257**: p. 2677-2682.
- 380 31. Raade, G., *Dypingite, a new hydrous basic carbonate of magnesium, from Norway*. The American  
381 Mineralogist, 1970. **88**: p. 1457.
- 382 32. White, W.B., *Infrared characterization of water and hydroxyl ion in the basic magnesium*  
383 *carbonate minerals*. American Mineralogist, 1971. **56**: p. 46-53.
- 384 33. Lanas, J. and J.I. Alvarez, *Dolomitic lime: thermal decomposition of nesquehonite*. Thermochemica  
385 Acta, 2004. **421**: p. 123-132.
- 386 34. Frost, R.L., S. Bahfenne, and J.E. Graham, *Raman spectroscopic study of the magnesium carbonate*  
387 *minerals- artinite and dypingite*. Journal of Raman Spectroscopy, 2009. **40**(8): p. 855-860.
- 388 35. Kontoyannis, C.G. and N.V. Vagenas, *Calcium carbonate phase analysis using XRD and FT-*  
389 *Raman spectroscopy*. The Analyst, 2000. **125**: p. 251-255.
- 390

1  
2 Table 1: Gibbs free energies of formation from the elements in their standard states at 298K for  
3 phases of interest to this work. [7, 8]

Phase	chemical composition	$\Delta G_f^0$ [kJ mol <sup>-1</sup> ]
Periclase	MgO	-566
Carbon dioxide (gas)	CO <sub>2</sub>	-394
Water (liquid)	H <sub>2</sub> O	-237
Brucite	Mg(OH) <sub>2</sub>	-835
Magnesite	MgCO <sub>3</sub>	-1028
Nesquehonite	MgCO <sub>3</sub> ·3H <sub>2</sub> O	-1724
Lansfordite	MgCO <sub>3</sub> ·5H <sub>2</sub> O	-2200
Artinite	MgCO <sub>3</sub> ·Mg(OH) <sub>2</sub> ·3H <sub>2</sub> O	-2569
Hydromagnesite	(MgCO <sub>3</sub> ) <sub>4</sub> ·Mg(OH) <sub>2</sub> ·4H <sub>2</sub> O	-5865
Calcite	CaCO <sub>3</sub>	-1129
Aragonite	CaCO <sub>3</sub>	-1128

5  
6  
7 Table 2: Chemical composition of MgO and hydromagnesite (HY) used in this study analysed  
8 by XRF using powder samples. The non-volatile elements (i.e. excluding CO<sub>2</sub> and H<sub>2</sub>O) are  
9 assumed to be present as oxides, totalling 100% on an ignited basis. Measured and expected  
10 1000°C ignition loss values are also given for the actual materials as used.

element	sample	
	HY	MgO
MgO	95.55	92.55
CaO	3.33	1.74
SiO <sub>2</sub>	0.47	2.72
Na <sub>2</sub> O	0.28	0.76
NiO	0.19	nd
Fe <sub>2</sub> O <sub>3</sub>	0.11	0.77
Al <sub>2</sub> O <sub>3</sub>	nd	1.02
SO <sub>3</sub>	0.07	0.44
LoI measured	55.60	2.0
LoI expected	56.90	0
BET surface area [m <sup>2</sup> /g]	n.a	30

nd = not detected

12  
13  
14

15  
 16 Table 3: Compressive strengths of paste samples at 7 and 28 days. Means and standard  
 17 deviations are calculated from 6 replicate measurements.

18

Time [days]	7		28	
MgO:HY ratio	strength	SD	strength	SD
	[MPa]		[MPa]	
9:1	17.3	0.8	24.6	0.6
8:2	17.1	0.9	23.8	0.7
7:3	17.3	1.0	24.5	0.4

19

20

21

22 Table 4: Summary of the bands detected and their origins, for the FTIR spectra in Fig.5.

23

<b>Band position (cm<sup>-1</sup>)</b>	<b>origin</b>	<b>movement</b>	<b>reference</b>
~ 600	Unknown	Unknown	[25, 26]
800 - 880	CO <sub>3</sub> <sup>2-</sup> from HY	Bending vibrations	[23, 30]
1120	CO <sub>3</sub> <sup>2-</sup> from HY	V <sub>1</sub> symmetric stretching vibration	[23, 30]
1420 - 1480	CO <sub>3</sub> <sup>2-</sup> / HCO <sub>3</sub> <sup>-</sup> from HY	V <sub>3</sub> asymmetric stretching vibration	[23, 24, 30]
1650 (shoulder)	H <sub>2</sub> O	Bending vibration	[31, 32]
3450, 3510	HY water of crystallisation		[23, 30]
3650	Mg(OH) <sub>2</sub> from HY	Free O-H vibration	[23, 33]
3700	Mg(OH) <sub>2</sub>	Anti-symmetrical O-H stretching vibration of lattice hydroxide	[22, 23]

24

25

26

27

28

29 Table 5: Bands summary of different hydrated magnesium carbonates as well as selected  
30 calcium carbonates in the region of 1200 - 1000  $\text{cm}^{-1}$  [28, 34, 35].

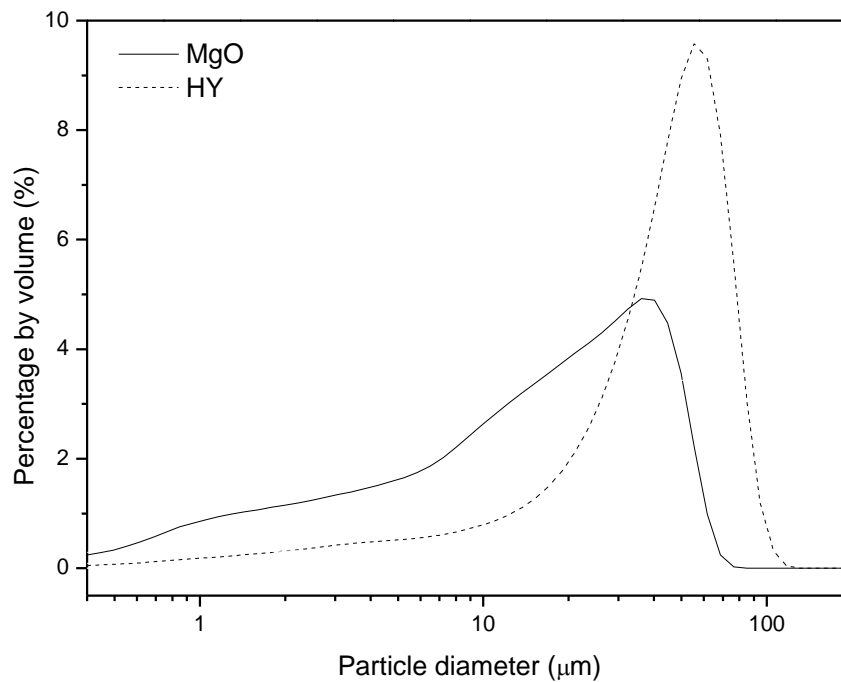
31

Mineral name	chemical formula	Wavenumber [ $\text{cm}^{-1}$ ]
Artinite	$\text{Mg}_2(\text{OH})_2\text{CO}_3 \cdot 3\text{H}_2\text{O}$	1092
Dypingite	$\text{Mg}_5(\text{CO}_3)_4(\text{OH})_2 \cdot 5\text{H}_2\text{O}$	1120
Dolomite	$\text{CaMg}(\text{CO}_3)_2$	1098
Huntite	$\text{Mg}_3\text{Ca}(\text{CO}_3)_4$	1123
Hydromagnesite	$\text{Mg}_5(\text{CO}_3)_4(\text{OH})_2 \cdot 4\text{H}_2\text{O}$	1119
Magnesite	$\text{MgCO}_3$	1094
Nesquehonite	$\text{Mg}(\text{HCO}_3)(\text{OH}) \cdot 2(\text{H}_2\text{O})$	1100
Calcite	$\text{CaCO}_3$	1084
Aragonite	$\text{CaCO}_3$	1084
Vaterite	$\text{CaCO}_3$	1089
-	$\text{HCO}_3^-$	1017
-	$\text{CO}_3^{2-}$	1065

32

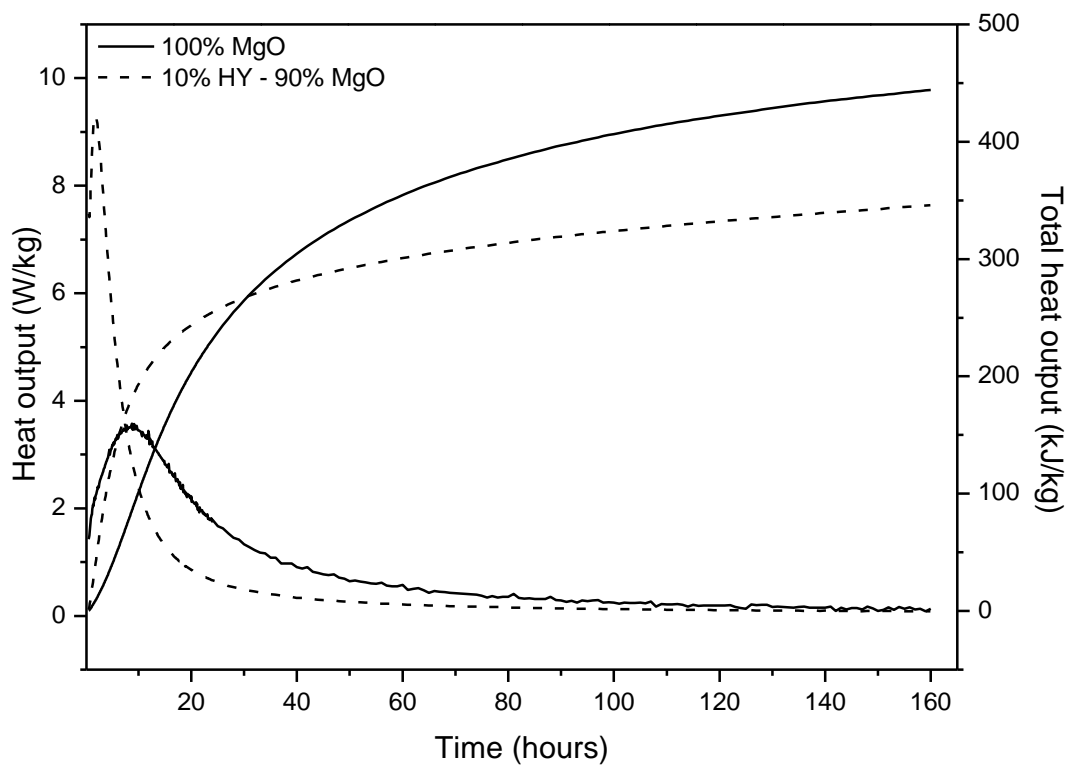
33

34



35

36 **Fig. 1.** Particle size distributions of the MgO and hydromagnesite (HY) used in this research.

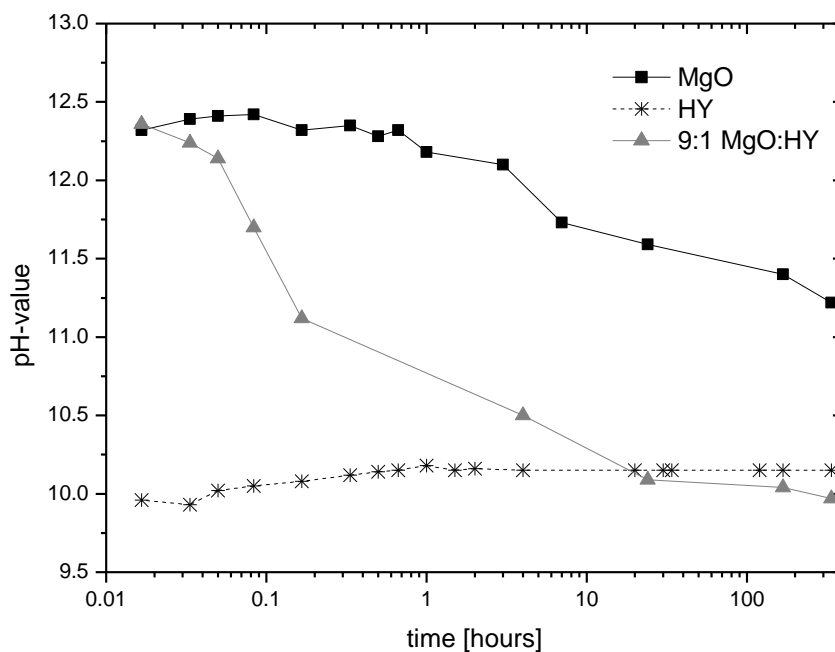


37

38 **Fig. 2.** Isothermal conduction calorimetry data for the pure MgO and 9:1 MgO: HY pastes.

39 Heat output is per kg of total sample mass.

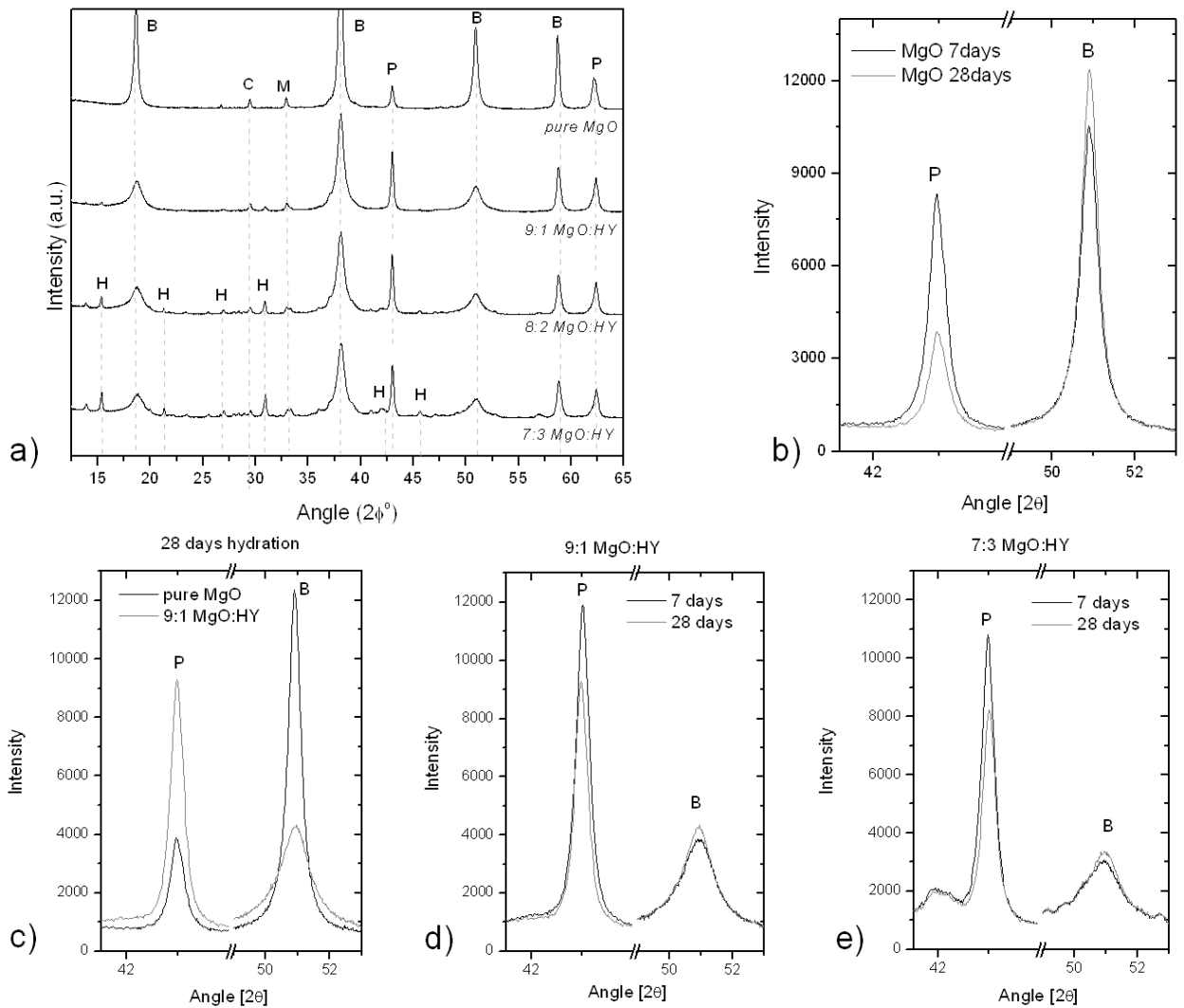




41

42 **Fig. 3.** Change in solution pH over time of w/s = 3 slurries containing 100% MgO, 100% HY  
43 and 10% HY - 90% MgO mixes. Each point represents the average of two measurements.

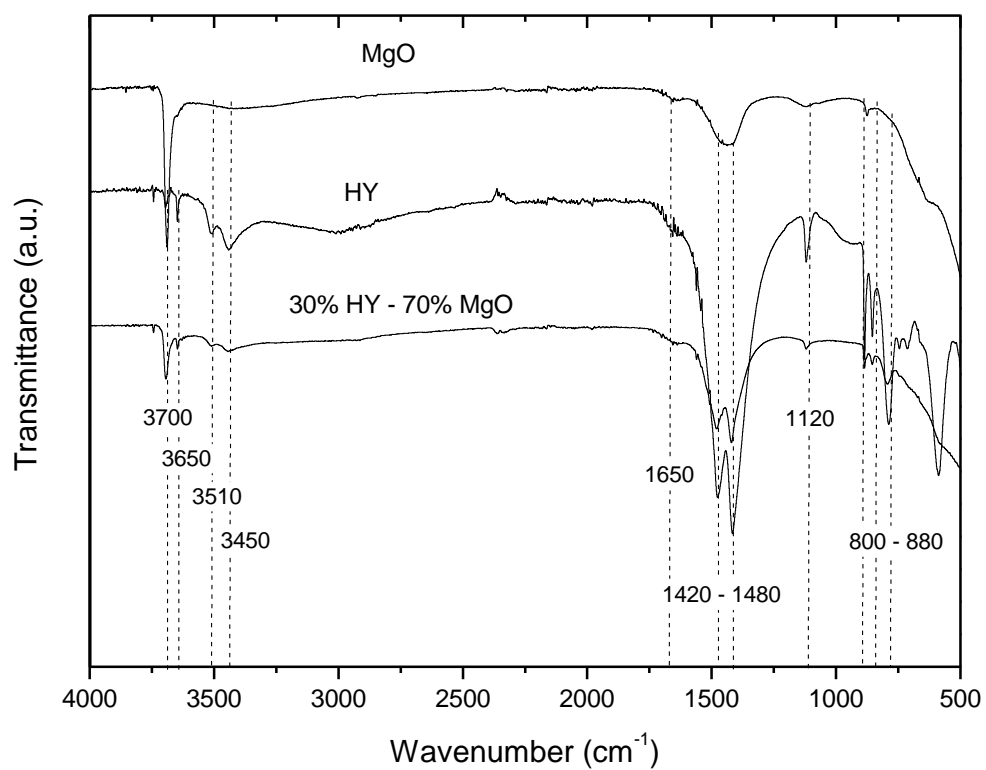
44



45

46 **Fig. 4.** Powder XRD scans of hydrated MgO and MgO-HY pastes made at 0.62 initial w/s  
 47 ratio. a) full scans of all four samples after 28 days curing; b) comparison of main periclase  
 48 and brucite peaks for pure MgO pastes at 7 and 28 days; c) Comparison of the main periclase  
 49 and brucite peaks for pure MgO and 9:1 MgO: HY mixture after 28 days; d) Comparison of  
 50 the main periclase and brucite peaks for the 9:1 MgO: HY mixture after 7 and 28 days; e)  
 51 Comparison of the main periclase and brucite peaks for the 7:3 MgO: HY mixture after 7 and  
 52 28 days. Key: B = brucite  $[\text{Mg}(\text{OH})_2]$ , C = calcite  $[\text{CaCO}_3]$ , H = hydromagnesite  
 53  $[\text{Mg}_5(\text{CO}_3)_4(\text{OH})_2 \cdot 4\text{H}_2\text{O}]$ , M = magnesite  $[\text{MgCO}_3]$  and P = periclase  $[\text{MgO}]$ .

54

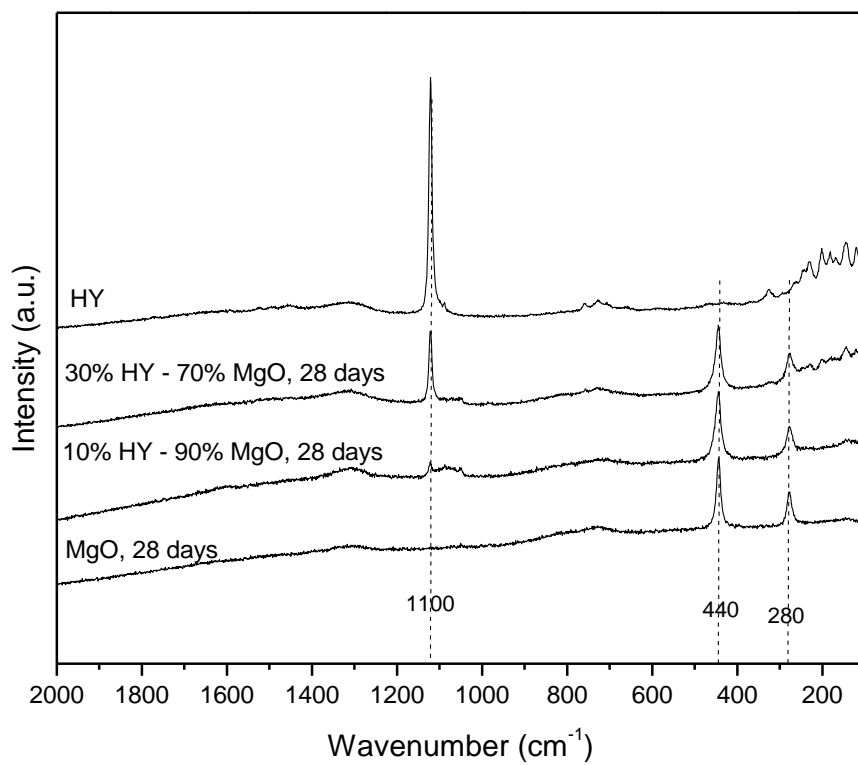


55

56

57 **Fig. 5.** FTIR spectra of pure MgO and 3:7 HY: MgO paste hydrated for 28 days, and HY as  
58 used. The peaks of interest are indicated with dotted lines and their wave number labelled.

59



60

61 **Fig. 6.** Raman spectra of the HY sample as used; plus the pastes of 3:7 and 9:1 HY: MgO  
62 blends, and pure MgO, hydrated for 28 days.

63

64

65

66

67

68

69

70

71

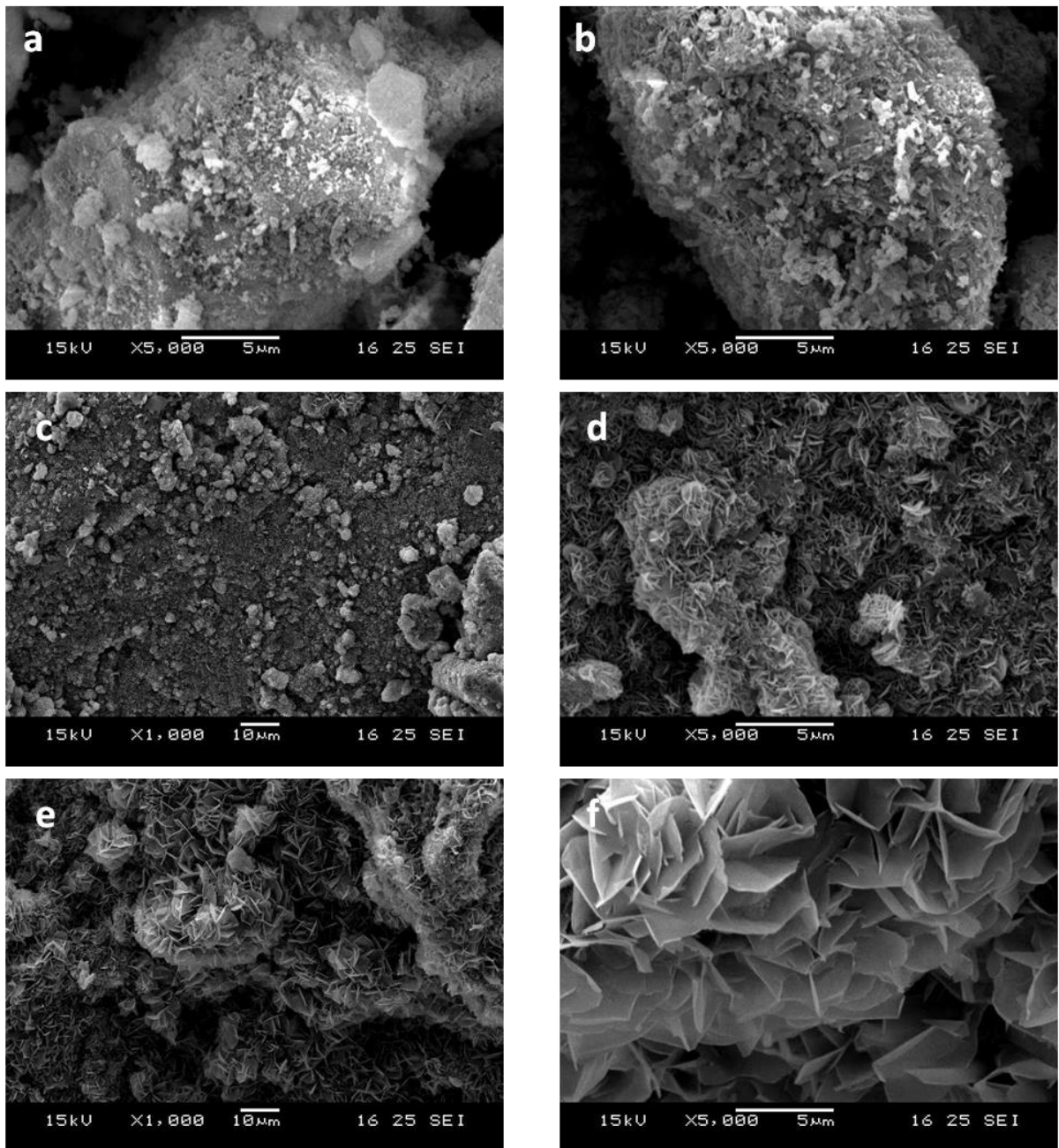
72

73

74

75

76



77

78

79 **Fig. 7.** SEM images of a) **as-received** MgO; b) **as-received** HY sample; c and d) 9:1 MgO:  
 80 HY pastes after 7 days hydration; e and f) 9:1 MgO: HY pastes after 28 days hydration.